α-MoO 3 Nanobelts: A High Performance Cathode Material for Lithium Ion Batteries

ARTICLE *in* THE JOURNAL OF PHYSICAL CHEMISTRY C · NOVEMBER 2010

Impact Factor: 4.77 · DOI: 10.1021/jp108778v · Source: OAI

α-MoO_3 Nanobelts: A High Performance Cathode Material for Lithium Ion Batteries

Liang Zhou,[||,†] Lichun Yang,[||,†] Pei Yuan,[†,‡] Jin Zou,[§] Yuping Wu,*[,†] and Chengzhong Yu*[,†,‡]

Department of Chemistry and Shanghai Key Laboratory of Molecular Catalysis and Innovative Materials, Fudan University, Shanghai 200433, People's Republic of China, ARC Centre of Excellence for Functional Nanomaterials and Australian Institute for Bioengineering and Nanotechnology, The University of Queensland, Brisbane, QLD 4072, Australia, and School of Engineering and Centre for Microscopy and Microanalysis, The University of Queensland, Brisbane, QLD 4072, Australia

Received: September 14, 2010; Revised Manuscript Received: October 27, 2010

Flexible single crystalline α-MoO_3 nanobelts with widths of 200−500 nm, lengths of 5−10 μm, and thicknesses of ∼50 nm have been prepared by a facile hydrothermal treatment method. When fabricated as the cathode for lithium ion batteries, the as-synthesized α-MoO_3 nanobelts exhibit excellent rate capability, large capacity, and good cycling stability. An initial discharge capacity of 176 mAh/g can be obtained at 5000 mA/g, retaining a capacity of 115 mAh/g after 50 cycles. The superior high-rate capability can be attributed to the increased conductivity of the electrode during cycling and the nanobelts morphology. The excellent performance makes the α-MoO_3 nanobelts a promising cathode material for rechargeable lithium ion batteries in the application of electronic vehicles and hybrid electronic vehicles.

Introduction

The lithium ion battery (LIB) is now prevailing in many portable electronic devices such as cell phones, digital cameras/videos, and laptop computers due to its longer cycling life and higher energy density than other rechargeable batteries.[1] Moreover, it has been extensively studied for use in new applications such as electronic vehicles (EVs), hybrid electronic vehicles (HEVs), and power backups, which require both high energy and high power densities. However, due to its relatively low specific power density (the ability to charge/discharge at very high rates), it is still difficult for LIBs to accomplish the industry needs of these new applications.[2] How to increase the specific power density of LIBs has recently become one of the most attractive topics of both scientific and industrial interests.[2−7] Recent studies show that changing the charges on the transition metal layers,[2] improving the Li^+ conductivity by surface coating,[3] enhancing the electron transport by employing either electron conductive core cable[8−11] or surface shell,[12−15] expanding the interlayer spacing,[16] and reducing the distance for Li^+ and electron diffusion by creating nanostructured materials[17−21] are several ideal ways to improve the rate performance of electrode materials.

Among all of the above-mentioned strategies, fabricating nanostructured electrode materials,[4−7] particularly one-dimensional (1D) nanowires/nanorods/nanobelts,[22−25] is considered to be the most promising avenue toward addressing rate limitations and satisfying the industrial goals. The 1D nanowires, nanorods, or nanobelts morphology not only has large electrode−electrolyte contact area and facile strain relaxation but also efficient 1D electron transport pathways.[22,23] As a result, 1D $LiMn_2O_4$,[22−24] V_2O_5,[25] Co_3O_4,[26,27] TiO_2(B),[28] $Li_{0.88}[Li_{0.18}Co_{0.33}Mn_{0.49}]O_2$,[29] $Li_{0.44}MnO_2$,[30] Fe_3O_4,[8] $FePO_4$,[10] and $Sn_{78}Ge_{22}$@carbon[11] nanowires have shown improved rate performances.

Molybdenum trioxide (MoO_3) is one of the most important catalysts for selective partial oxidation in modern industry.[31,32] It is also a promissing material in photochromic and electrochromic devices,[33,34] field emission,[35] gas sensors,[36] and energy storage.[16,37−40] There are three basic polymorphs of MoO_3, i.e., orthorhombic MoO_3 (α-MoO_3), monoclinic MoO_3 (β-MoO_3), and hexagonal MoO_3, in which α-MoO_3 is the thermodynamically stable phase.[38,41] The α-MoO_3 phase possesses a unique layered structure: each layer is composed of two sublayers which are formed by corner-sharing [MoO_6] octahedra along [001] and [100] directions, and two sublayers are stacked together by sharing the edges of octahedra along the [001] direction. An alternate stacking of these layers along the [010] direction with van der Waals interaction leads to the formation of α-MoO_3 with a two-dimensional structure (Figure S1, Supporting Information) which allows guest atoms, ions (such as Li^+), or molecules to be introduced between the layers through intercalation. As one of the earliest studied host materials for lithium ion insertion, α-MoO_3 can accommodate ca. 1.5 lithium per molybdenum atom,[42,43] and lithiated MoO_3 (Li_xMoO_3) was found to have good electronic conductivity and high Li^+ mobility.[16,44] Although α-MoO_3 microrods,[45] nanobelts,[16,46−49] and nanoparticles[37,50] have been employed in LIBs and some of them show high capacity and good cycling stability, most of these works are performed under low current densities. To the best of our knowledge, the highest current density for α-MoO_3 cathodes employed in previous literature is 400 mA/g,[46] and that applied to α-MoO_3 anodes is ∼2 C (∼1000 mA/g).[37]

In this article, we report the hydrothermal synthesis and high-rate performance of α-MoO_3 nanobelts. The as-synthesized single-crystalline α-MoO_3 nanobelts exhibit excellent rate capability, large capacity, and cycling stability. The excellent

* To whom correspondence should be addressed, c.yu@uq.edu.au and wuyp@fudan.edu.cn.
[||] These authors contributed equally to this paper.
[†] Department of Chemistry and Shanghai Key Laboratory of Molecular Catalysis and Innovative Materials, Fudan University.
[‡] ARC Centre of Excellence for Functional Nanomaterials and Australian Institute for Bioengineering and Nanotechnology, The University of Queensland.
[§] School of Engineering and Centre for Microscopy and Microanalysis, The University of Queensland.

10.1021/jp108778v
Published on Web 11/15/2010

performance makes the α-MoO_3 nanobelts a promising cathode material for rechargeable LIBs in the application of EVs and HEVs.

Experimental Section

Preparation. The α-MoO_3 nanobelts were synthesized by hydrothermal treatment of a peroxomolybdic acid solution. The peroxomolybdic acid precursor solution was prepared as follows: 80 mL of 30 wt % H_2O_2 aqueous solution was slowly added to a round bottle flask containing of 9.6 g of Mo metal powder in an icy water bath with violent magnetic stirring. A transparent yellow solution was obtained, and it was further diluted to 0.10 mol/L. In a typical synthesis of MoO_3 paper, 30 mL of precursor solution was sealed in a 200 mL autoclave and hydrothermally treated at 180 °C for 24 h. A white colloidal suspension was obtained; the MoO_3 paper was prepared by vacuum filtration and washed thoroughly with distilled water.

Characterization. X-ray diffraction (XRD) measurements were performed on a German Bruker D4 X-ray diffractometer with Ni-filtered Cu Kα radiation. Transmission electron microscopy (TEM) images were taken on a JEOL 2011 microscope operated at 200 kV and a FEI Tecnai F30 microscope operated at 300 kV. Scanning electron microscopy (SEM) images were obtained on a Philips XL30 microscope operated at 20 kV.

Electrochemical Measurements. The electrochemical performance of the as-obtained MoO_3 was tested as the cathode for a rechargeable lithium battery. The electrode was prepared by pressing a powder mixture of MoO_3, acetylene black, and poly(tetrafluoroethylene) (PTFE) in a weight ratio of 80:10:10 onto a Ni grid. Model button cells were assembled in a glovebox with lithium foil as the counter and reference electrodes, Celgard 2400 as the separator, and LIB315 (a standard 1 mol/L $LiPF_6$ solution in a 1:1:1 mixture of EC, DMC, and DEC, Guotai Huarong Chemical Plant) as the electrolyte. Cyclic voltammetry was measured using a CHI 600C electrochemical workstation (Shanghai CH Instruments). Galvanostatic cycling was performed using a LANDct3.3 battery tester.

Results and Discussion

α-MoO_3 nanobelts were synthesized by hydrothermal treatment of a peroxomolybdic acid solution which has been demonstrated to be a facile method for the preparation of α-MoO_3 nanobelts.[51−55] MoO_3 papers can be fabricated by vacuum filtration of the α-MoO_3 nanobelts suspension. The size and thickness of the paper can be controlled by varying the size of the Buchner funnel and the quantity of the α-MoO_3 nanobelt suspension. A digital photograph of as-prepared free-standing MoO_3 paper peeled off a filter paper is shown in Figure 1a. The paper is flexible and can be bent without breaking-off (inset of Figure 1a). Such paper-like materials composed of one-dimensional transition metal oxide nanowires/nanobelts have wide potential applications in gas sensors, supercapacitors, actuators, and environmental remediations.[56−58]

The XRD pattern of α-MoO_3 paper is shown in Figure 1b. All diffraction peaks can be exclusively indexed as the orthorhombic MoO_3 phase (commonly denoted as α-MoO_3) with lattice parameters of $a = 0.3963$ nm, $b = 1.3856$ nm, and $c = 0.3697$ nm and a space group of *Pbnm* (Joint Committee on Powder Diffraction Standards, JCPDS No. 35-0609), suggesting a high purity of the products. The strong intensities of 020*, 040*, and 060* diffraction peaks indicate that there is a preferred orientation of the α-MoO_3 nanobelts with most α-MoO_3 nanobelts lying flat on the *ac* plane in the paper. Panels c and d of Figure 1 present the top- and side-view SEM images of

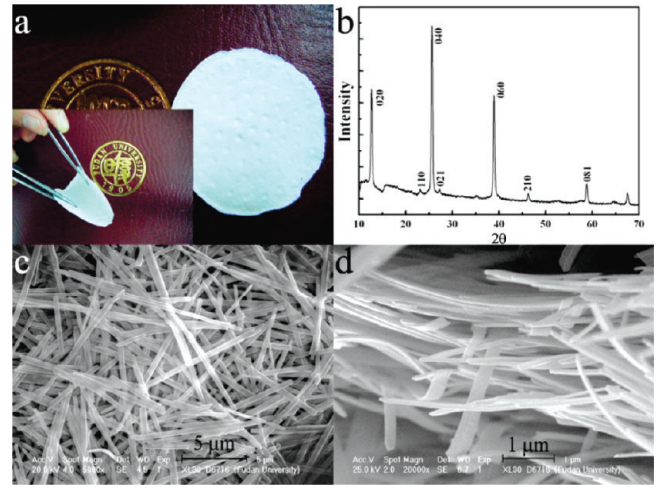

Figure 1. Digital photographs (a) and XRD pattern (b) of free-standing MoO_3 paper. SEM images viewed from top (c) and side (d) of as-prepared α-MoO_3 nanobelts, respectively.

α-MoO_3 nanobelts, respectively. Uniform α-MoO_3 nanobelts with width of ∼200−500 nm and lengths of ∼5−10 μm can be observed clearly. However, the thicknesses of the nanobelts are hard to determine from the SEM images. From Figure 1d, it is also found that some α-MoO_3 nanobelts can bend with large angles, which explains the flexibility of free-standing MoO_3 paper.

To further understand the morphology and structure characteristics of α-MoO_3 nanobelts, TEM was employed. Figure 2a presents a typical TEM image which further confirms the overall beltlike morphology of as-prepared products. A top-view TEM image of two parallel well-developed α-MoO_3 nanobelts and corresponding selected area electron diffraction (SAED) pattern are shown in panels b and c of Figure 2, respectively. From the contrast along the width of the nanobelts (refer to Figure 2b), it is obvious that the observed nanobelts are actually composed of two parallel and closely stacked single nanobelts. It is of interest to note that, although the observed nanobelts are composed of two single nanobelts, only one set of electron diffraction spots can be detected, indicating that two parallel nanobelts have identical crystallographic orientation. The most possible reason for this phenomenon is "oriented attachment". The SAED pattern shown in Figure 2c can be attributed to the [010] zone axis of orthorhombic α-MoO_3. It should be mentioned that, besides the allowed diffraction spots such as 200* and 002*, some forbidden diffraction spots can also be observable (such as 100* and 001* indicated by white arrows), which can be explained as the double diffraction caused by the dynamic scattering of the strong electron beam. On comparison of the TEM image and its corresponding SAED pattern, it is confirmed that the α-MoO_3 nanobelts grow along the [001] direction. Two sets of crystal lattice fringes, corresponding to the {100} (0.40 nm) and {001} (0.37 nm) atomic spacings, can be clearly distinguished in the top-view high-resolution (HR) TEM image of the α-MoO_3 nanobelt (Figure 2d). A TEM image showing both side-standing and flat-lying nanobelts on the copper grid is presented in Figure 2e inset. The side-standing nanobelt (Figure 2e and Figure S2 in the Supporting Information) has a thickness of ca. ∼50 nm. Bent contours can be clearly detected in Figure 2e inset (indicated by black arrows), which indicates the high crystallinity and thin characteristics of the α-MoO_3 nanobelts. The SAED pattern of the side-standing nanobelt shown in Figure 2e is shown in Figure 2f. The set of diffraction spots can be indexed to the [100] zone axis of the

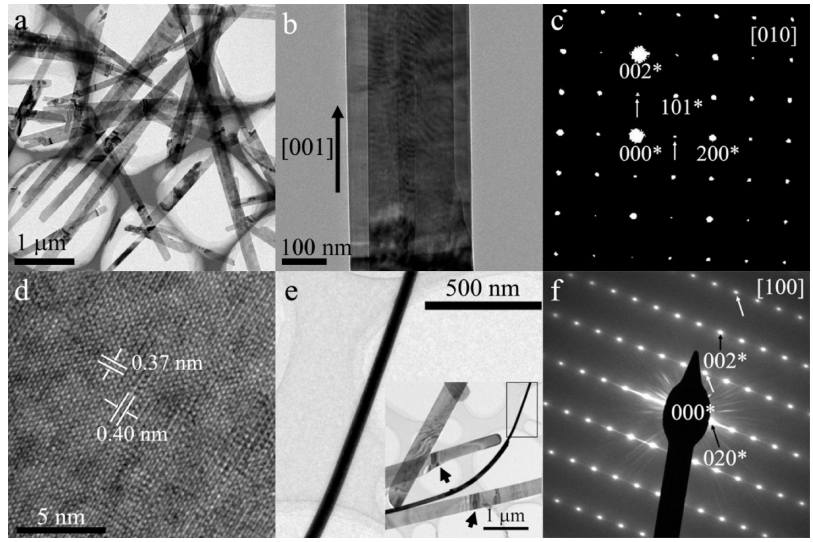

Figure 2. Overall TEM image (a), a top-view TEM image (b) and the corresponding ED pattern (c), a top-view HRTEM image (d), a side-view TEM image taken from the rectangle region of inset showing both side-standing and flat-lying nanobelts (e), and the corresponding ED pattern (f).

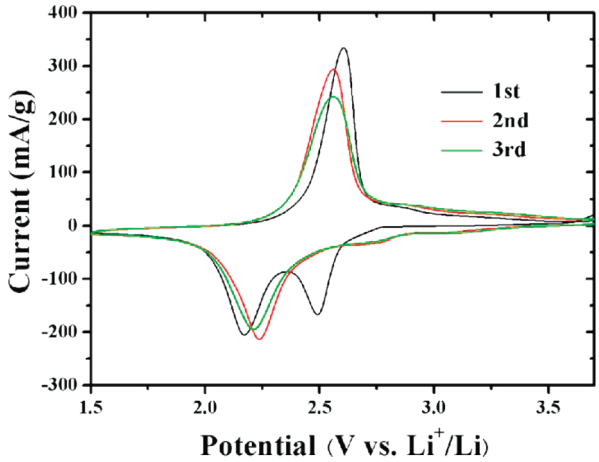

Figure 3. CVs of the electrodes made from the α-MoO_3 nanobelts in the first, second, and third cycles at a scan rate of 0.5 mV s^{-1}.

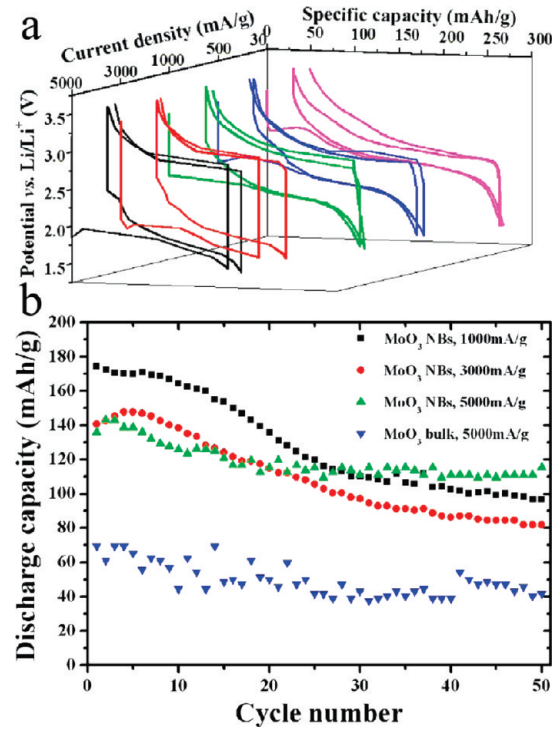

Figure 4. Discharge/charge curves as a function of capacity at different current densities in the initial two cycles (a) and cycling behavior of the electrodes made from α-MoO_3 nanobelts tested in the range of 1.5−3.5 V vs Li^+/Li at different current densities (b).

orthorhombic α-MoO_3, confirming that the side-standing nanobelt is standing on the {100} plane. Again, some forbidden diffraction spots caused by "double diffraction" can be detected (indicated by white arrows).

The as-prepared α-MoO_3 nanobelts were tested as cathode materials for a rechargeable lithium battery. Figure 3 shows the cyclic voltammograms (CVs) of the electrode made of α-MoO_3 nanobelts in the initial three consecutive cycles. In the cathodic polarization process of the first cycle, two strong peaks are observed at 2.49 and 2.17 V vs Li^+/Li. However, in the following anodic polarization, there is only one peak located at around 2.60 V. Similar CVs have also been reported by Chen et al.[46] It has been reported that the lithium ions can insert not only into the interlayer spacing between the [MoO_6] octahedron layers but also into the [MoO_6] octahedron intralayers.[45] The prominent set of peaks (2.17/2.60 V) in our case corresponds to the reversible insertion/deinsertion of lithium ions in the interlayer spacings (van der Waals spacings) between the [MoO_6] octahedron layers, and this set of peaks was found to be at (2.10/2.55 V) in Li et al.'s study.[45] For the cathodic peak at 2.49 V, it can be assigned to the irreversible lithium insertion into the crystal structure (probably into the [MoO_6] intralayers), which tends to trigger unrecoverable structural transformation of α-MoO_3.[45,46] The separation between the redox couple is small and the CV curves for the second and third cycles generally overlap, suggesting the good reversibility of lithium ion insertion/extraction in the van der Waals spacings of α-MoO_3 nanobelts.

Figure 4a shows the discharge/charge curves of the α-MoO_3 nanobelts at various current densities from 30 to 5000 mA/g. In the discharge curve recorded under 30 mA/g between 1.5 and 3.5 V, there are two plateaus, in accordance with the cathodic peaks in the CV for the first cycle (Figure 3). Under higher current densities, the polarization is serious: the difference between the two plateaus becomes inconspicuous and the hysteresis in the discharge/charge profiles becomes larger. The α-MoO_3 nanobelt electrode delivers a discharge capacity of 264 mAh/g at a current density of 30 mA/g, corresponding to the

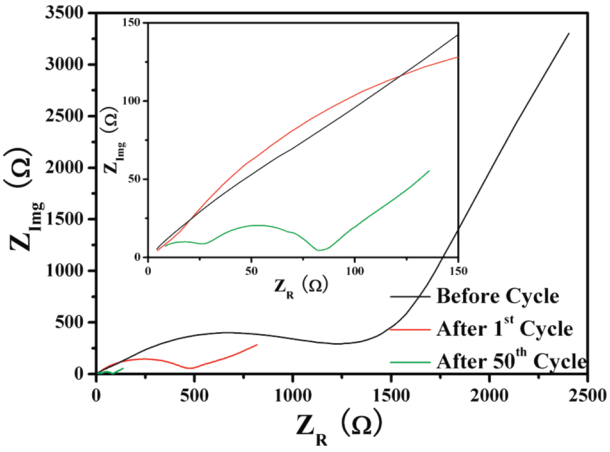

Figure 5. Nyquist plots of α-MoO_3 nanobelt electrode before cycle at the open circuit voltage 3.2 V and after first and 50th cycle (discharge/charge at a current density of 3000 mA g^{-1} in the range of 1.5−3.5 V vs Li^+/Li) at a discharge potential of 3.2 V vs. Li^+/Li at 25 °C from 100 kHz to 10 mHz. The inset is the magnification of the plots at high frequency.

intercalation of 1.42 Li^+ per formula of MoO_3. During the consecutive charge process, a charge capacity of 235 mAh/g is achieved, corresponding to the deintercalation of 1.26 Li^+ per formula of MoO_3. Even when the current density increases to 5000 mA/g, it retains a capacity as high as 176 mAh/g, 66.4% of that under 30 mA/g, which is rarely reported to our knowledge. Although the discharge voltage plateau drops to 2.0−1.6 V at a current density of 5000 mA/g, the power density still reaches 9000 W/kg with the high energy density of >300 W h/kg. The cycling performance under high current densities is shown in Figure 4b. After 50 cycles of discharge/charge at 5000 mA/g, the α-MoO_3 nanobelt electrode still preserves a capacity of 114 mAh/g, 65% of its initial cycle. However, under the same condition, bulk α-MoO_3 (about 10 μm in size) only gives a capacity less than 70 mAh/g. As a cathode material, α-MoO_3 nanobelts show higher capacity and better cycle ability in the high rate performance over bulk α-MoO_3.

The Coulombic efficiency versus cycle number under different current densities is shown in Figure S3 (Supporting Information). For the first discharge−charge cycle at 5000 mA/g, a relatively low Coulombic efficiency of ~74% is achieved, which indicates the deintercalation of Li^+ is incomplete (ca. 0.25 Li^+ is trapped per MoO_3). After the first cycle, the cell maintained a high Coulombic efficiency between 96 and 101% for the remaining 49 cycles. Similar trends can also be found for current densities of 1000 and 3000 mA/g.

To understand the superior high rate performance of α-MoO_3 nanobelts, we measured the electrochemical impedance spectroscopy (EIS) of the α-MoO_3 nanobelt electrode. Figure 5 shows the Nyquist plots of the same α-MoO_3 nanobelt electrode before and after cycles. Apparent semicircles are observed in the high-frequency region, which can be assigned to the charge-transfer impedance at the interface between the electrolyte and the working electrode. By extrapolating a semicircle of Figure 5, two values can be obtained in the real axis at which the plot intercepts with the axis. The value at the high-frequency side turns out to give the solution resistance; the low-frequency one gives the solution resistance together with the charge-transfer resistance. Subtracting the solution resistance, the charge-transfer resistance is obtained. From the figure, it can be seen that the charge-transfer resistance decreases after the first cycle and become even smaller after the 50th cycle. The increase of the

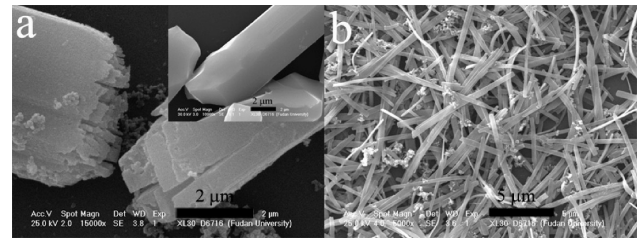

Figure 6. SEM image of (a) bulk α-MoO_3 and (b) α-MoO_3 nanobelts after 50 cycles of discharge/charge at a current density of 5000 mA/g in the potential range of 1.5−3.5 V vs Li/Li^+. The inset of Figure 6 is the SEM image of bulk α-MoO_3 before cycling. After the discharge/charge process, bulk α-MoO_3 is ruptured while α-MoO_3 nanobelts preserve their morphology.

conductivity of the electrode can be attributed to the incomplete deintercalation of Li^+ during cycling (ca. 0.25 Li^+ is trapped in per formula of MoO_3 at 5000 mA/g), which results in the formation of Li_xMoO_3 with better conductivity when compared to pristine α-MoO_3.[16,44] The Li_xMoO_3 facilitates a charge-transfer reaction on the electrolyte/electrode interface as well as Li^+ diffusion in the electrode, therefore beneficial for the high rate performance.

Besides the increased conductivity of the electrode after the discharge/charge process, the excellent high rate performance is highly related to the nanobelt morphology of the α-MoO_3 cathode material. It has been demonstrated that lithium ion insertion/deinsertion takes place in the van der Waals spacings which is parallel to the *ac* plane.[45] For our α-MoO_3 nanobelts, the diffusion distance for Li^+ ions is only half of its width (100−250 nm), which is greatly decreased compared with bulk α-MoO_3 and thus mitigates the slow solid-state diffusion. Meanwhile, α-MoO_3 nanobelts have a large surface area which would reduce the actual effective current density on the active material and relief the strain induced by the volume change during the electrochemical reaction. Moreover, due to the flexibility of the α-MoO_3 nanobelts, the morphology of α-MoO_3 nanobelts can be preserved during the Li^+ insertion/extraction process even under a current density of 5000 mA/g for 50 cycles (Figure. 6b), while the bulk α-MoO_3 cracks during the same process (Figure 6a). In addition, under high current densities, due to the serious polarization, insertion into the [MoO_6] octahedron intralayers may be mitigated; thus the unrecoverable structural transition can be depressed. As a result, the α-MoO_3 nanobelts can achieve good cycling stability and high rate capability.

Conclusion

In conclusion, single crystalline α-MoO_3 nanobelts have been successfully synthesized through a hydrothermal method and tested as cathode material for a rechargeable lithium battery. The α-MoO_3 nanobelts exhibit a high discharge capacity of 264 mAh/g at 30 mA/g and 176 mAh/g at 5000 mA/g. The capacity is still up to 114 mAh/g after 50 cycles at the high current density of 5000 mA/g. The increased conductivity of the electrode during cycling and the nanobelt morphology are responsible for the superior high-rate capability. This excellent high rate performance makes α-MoO_3 nanobelts promising cathode materials for rechargeable lithium batteries in the application of HEVs and EVs.

Acknowledgment. This research was financially supported by the Sate Key Research Program (2010CB226901, 2007CB209702),

NSFC (20721063), STC of Shanghai (08DZ2270500), and the Australian Research Council.

Supporting Information Available: Structure model of α-MoO_3, TEM image of α-MoO_3 nanobelts, Coulombic efficiency versus cycle number, and safety issues. This material is available free of charge via the Internet at http://pubs.acs.org.

References and Notes

(1) Tarascon, J. M.; Armand, M. *Nature* **2001**, *414*, 359–367.
(2) Kang, K. S.; Meng, Y. S.; Breger, J.; Grey, C. P.; Ceder, G. *Science* **2006**, *311*, 977–980.
(3) Kang, B.; Ceder, G. *Nature* **2009**, *458*, 190–193.
(4) Guo, Y. G.; Hu, J. S.; Wan, L. J. *Adv. Mater.* **2008**, *20*, 2878–2887.
(5) Wang, Y.; Cao, G. Z. *Adv. Mater.* **2008**, *20*, 2251–2269.
(6) Bruce, P. G.; Scrosati, B.; Tarascon, J. M. *Angew. Chem., Int. Ed.* **2008**, *47*, 2930–2946.
(7) Arico, A. S.; Bruce, P.; Scrosati, B.; Tarascon, J. M.; Van Schalkwijk, W. *Nat. Mater.* **2005**, *4*, 366–377.
(8) Taberna, L.; Mitra, S.; Poizot, P.; Simon, P.; Tarascon, J. M. *Nat. Mater.* **2006**, *5*, 567–573.
(9) Magasinski, A.; Dixon, P.; Hertzberg, B.; Kvit, A.; Ayala, J.; Yushin, G. *Nat. Mater.* **2010**, *9*, 353–358.
(10) Lee, Y. J.; Yi, H.; Kim, W. J.; Kang, K.; Yun, D. S.; Strano, M. S.; Ceder, G.; Belcher, A. M. *Science* **2009**, *324*, 1051–1055.
(11) Lee, H.; Cho, J. *Nano Lett.* **2007**, *7*, 2638–2641.
(12) Wang, Y. G.; Wang, Y. R.; Hosono, E. J.; Wang, K. X.; Zhou, H. S. *Angew. Chem., Int. Ed.* **2008**, *47*, 7461–7465.
(13) Wu, X. L.; Jiang, L. Y.; Cao, F. F.; Guo, Y. G.; Wan, L. J. *Adv. Mater.* **2009**, *21*, 2710–2714.
(14) Guo, Y. G.; Hu, Y. S.; Sigle, W.; Maier, J. *Adv. Mater.* **2007**, *19*, 2087–2091.
(15) Hu, Y. S.; Guo, Y. G.; Dominko, R.; Gaberscek, M.; Jamnik, J.; Maier, J. *Adv. Mater.* **2007**, *19*, 1963–1966.
(16) Mai, L. Q.; Hu, B.; Chen, W.; Qi, Y. Y.; Lao, C. S.; Yang, R. S.; Dai, Y.; Wang, Z. L. *Adv. Mater.* **2007**, *19*, 3712–3716.
(17) Okubo, M.; Hosono, E.; Kim, J.; Enomoto, M.; Kojima, N.; Kudo, T.; Zhou, H. S.; Honma, I. *J. Am. Chem. Soc.* **2007**, *129*, 7444–7452.
(18) Chen, H. L.; Grey, C. P. *Adv. Mater.* **2008**, *20*, 2206–2210.
(19) Okubo, M.; Mizuno, Y.; Yamada, H.; Kim, J.; Hosono, E.; Zhou, H. S.; Kudo, T.; Honma, I. *ACS Nano* **2010**, *4*, 741–752.
(20) Jiao, F.; Bao, J. L.; Hill, A. H.; Bruce, P. G. *Angew. Chem., Int. Ed.* **2008**, *47*, 9711–9716.
(21) Ren, Y.; Armstrong, A. R.; Jiao, F.; Bruce, P. G. *J. Am. Chem. Soc.* **2010**, *132*, 996–1004.
(22) Hosono, E.; Kudo, T.; Honma, I.; Matsuda, H.; Zhou, H. S. *Nano Lett.* **2009**, *9*, 1045–1051.
(23) Kim, D. K.; Muralidharan, P.; Lee, H. W.; Ruffo, R.; Yang, Y.; Chan, C. K.; Peng, H.; Huggins, R. A.; Cui, Y. *Nano Lett.* **2008**, *8*, 3948–3952.
(24) Yang, Y.; Xie, C.; Ruffo, R.; Peng, H. L.; Kim, D. K.; Cui, Y. *Nano Lett.* **2009**, *9*, 4109–4114.
(25) Chan, C. K.; Peng, H. L.; Twesten, R. D.; Jarausch, K.; Zhang, X. F.; Cui, Y. *Nano Lett.* **2007**, *7*, 490–495.
(26) Nam, K. T.; Kim, D. W.; Yoo, P. J.; Chiang, C. Y.; Meethong, N.; Hammond, P. T.; Chiang, Y. M.; Belcher, A. M. *Science* **2006**, *312*, 885–888.
(27) Li, Y. G.; Tan, B.; Wu, Y. Y. *Nano Lett.* **2008**, *8*, 265–270.
(28) Armstrong, G.; Armstrong, A. R.; Bruce, P. G.; Reale, P.; Scrosati, B. *Adv. Mater.* **2006**, *18*, 2597–2600.
(29) Lee, Y. J.; Kim, M. G.; Cho, J. *Nano Lett.* **2008**, *8*, 957–961.
(30) Hosono, E.; Matsuda, H.; Saito, T.; Kudo, T.; Ichihara, M.; Honma, I.; Zhou, H. S. *J. Power Sources* **2010**, *195*, 7098–7101.
(31) Sadakane, M.; Watanabe, N.; Katou, T.; Nodasaka, Y.; Ueda, W. *Angew. Chem., Int. Ed.* **2007**, *46*, 1493–1496.
(32) Tsuji, H.; Koyasu, Y. *J. Am. Chem. Soc.* **2002**, *124*, 5608–5609.
(33) Yao, J. N.; Hashimoto, K.; Fujishima, A. *Nature* **1992**, *355*, 624–626.
(34) Zheng, L.; Xu, Y.; Jin, D.; Xie, Y. *Chem. Mater.* **2009**, *21*, 5681–5690.
(35) Zhou, J.; Xu, N. S.; Deng, S. Z.; Chen, J.; She, J. C.; Wang, Z. L. *Adv. Mater.* **2003**, *15*, 1835–1840.
(36) Comini, E.; Yubao, L.; Brando, Y.; Sberveglieri, G. *Chem. Phys. Lett.* **2005**, *407*, 368–371.
(37) Lee, S. H.; Kim, Y. H.; Deshpande, R.; Parilla, P. A.; Whitney, E.; Gillaspie, D. T.; Jones, K. M.; Mahan, A. H.; Zhang, S. B.; Dillon, A. C. *Adv. Mater.* **2008**, *20*, 3627–3632.
(38) Chernova, N. A.; Roppolo, M.; Dillon, A. C.; Whittingham, M. S. *J. Mater. Chem.* **2009**, *19*, 2526–2552.
(39) Zheng, L.; Xu, Y.; Jin, D.; Xie, Y. *J. Mater. Chem.* **2010**, *20*, 7135–7143.
(40) Brezesinski, T.; Wang, J.; Tolbert, S. H.; Dunn, B. *Nat. Mater.* **2010**, *9*, 146–151.
(41) Lou, X. W.; Zeng, H. C. *Chem. Mater.* **2002**, *14*, 4781–4789.
(42) Whittingham, M. S. *J. Electrochem. Soc.* **1976**, *123*, 315–320.
(43) Dampier, F. W. *J. Electrochem. Soc.* **1974**, *121*, 656–660.
(44) Julien, C.; Nazri, G. A. *Solid State Ion.* **1994**, *68*, 111–116.
(45) Li, W. Y.; Cheng, F. Y.; Tao, Z. L.; Chen, J. *J. Phys. Chem. B* **2006**, *110*, 119–124.
(46) Chen, J. S.; Cheah, Y. L.; Madhavi, S.; Lou, X. W. *J. Phys. Chem. C* **2010**, *114*, 8675–8678.
(47) Reddy, C. V. S.; Walker, E. H.; Wen, C.; Mho, S. I. *J. Power Sources* **2008**, *183*, 330–333.
(48) Reddy, C. V. S.; Deng, Z. R.; Zhu, Q. Y.; Dai, Y.; Zhou, J.; Chen, W.; Mho, S. I. *Appl. Phys. A: Mater. Sci. Process.* **2007**, *89*, 995–999.
(49) Hassan, M. F.; Guo, Z. P.; Chen, Z.; Liu, H. K. *J. Power Sources* **2010**, *195*, 2372–2376.
(50) Riley, L. A.; Lee, S. H.; Gedvilias, L.; Dillon, A. C. *J. Power Sources* **2010**, *195*, 588–592.
(51) Hu, X. K.; Ma, D. K.; Xu, L. Q.; Zhu, Y. C.; Qian, Y. T. *Chem. Lett.* **2006**, *35*, 962–963.
(52) Hu, B.; Mai, L. Q.; Chen, W.; Yang, F. *ACS Nano* **2009**, *3*, 478–482.
(53) Li, G. C.; Jiang, L.; Pang, S. P.; Peng, H. R.; Zhang, Z. K. *J. Phys. Chem. B* **2006**, *110*, 24472–24475.
(54) Xia, T.; Li, Q.; Liu, X. D.; Meng, J.; Cao, X. Q. *J. Phys. Chem. B* **2006**, *110*, 2006–2012.
(55) Fang, L.; Shu, Y. Y.; Wang, A. Q.; Zhang, T. *J. Phys. Chem. C* **2007**, *111*, 2401–2408.
(56) Wang, Y. M.; Du, G. J.; Liu, H.; Liu, D.; Qin, S. B.; Wang, N.; Hu, C. G.; Tao, X. T.; Jiao, J.; Wang, J. Y.; Wang, Z. L. *Adv. Funct. Mater.* **2008**, *18*, 1131–1137.
(57) Gu, G.; Schmid, M.; Chiu, P. W.; Minett, A.; Fraysse, J.; Kim, G. T.; Roth, S.; Kozlov, M.; Munoz, E.; Baughman, R. H. *Nat. Mater.* **2003**, *2*, 316–319.
(58) Yuan, J. K.; Liu, X. G.; Akbulut, O.; Hu, J. Q.; Suib, S. L.; Kong, J.; Stellacci, F. *Nat. Nanotechnol.* **2008**, *3*, 332–336.

JP108778V